On the Mechanics and Physics in the Nano-Indentation of Silicon Monocrystals*

Liang-Chi ZHANG** and Hiroaki TANAKA**

This paper aims to investigate some fundamental problems of mechanics and physics in the nano-indentation of silicon monocrystals with the aid of molecular dynamics analysis. The study showed that inelastic deformation of silicon monocrystals is solely caused by amorphous phase transformation. Dislocations do not appear and purely elastic deformation exists only in an extremely narrow regime. The onset of inelastic deformation can be predicted by a criterion considering either the octahedral or maximum shear stress. Due to phase transformation, the contact area between indenter and specimen varies in a very complex manner. The study offers a new theory for the nano-indentation of monocrystalline silicon.

Key Words: Nano-Indentation, Silicon, Physics, Mechanics, Stress Criterion, Phase Transformation, Contact Area, Molecular Dynamics.

1. Introduction

Silicon monocrystals are important materials for semiconductor devices, high density information storage devices and micro-electro-mechanical systems. The fabrication and application of these delicate devices demand that a high surface integrity must be achieved by ultra-precision machining and a stable property of tribology must be maintained. These in turn require that the mechanical behaviour of a silicon monocrystal subjected to various loading conditions needs to be fully understood.

Indentation mechanics has been well developed and widely used to characterize the constitutive behaviour of metals in various engineering fields[1]. In recent years, in has also been regarded as a suitable method for understanding the mechanical behaviour of hard and brittle materials, such as ceramics, glass and silicon, whose properties are difficult to characterize by conventional techniques, such as the simple tensile test, because of their brittle nature[2]-[7]. With the recent emergence of ultra-precision machining[8] and micro/nano-tribology[9]-[11], the theory and technique of micro/nano-indentation have attracted greater and greater attention[12]-[18].

There are some fundamental problems in characterising the properties of a silicon monocrystal by nano-indentation. First, an experimental result may not represent the true behaviour of the material, because surface roughness, surface contamination, surface microstructural change, subsurface microcracks and profile accuracy of the indenter may all affect the response of silicon under indentation on the nanometre scale. Zhang, Tanaka and Zarudi[19] has pointed out that a specimen of a silicon monocrystal prepared by grinding and polishing normally contains an amorphous surface layer of SiO_x, about 10 to 80 nm thick, followed by a region with dislocations. Hence, tests using such specimens cannot provide exact information about a true silicon monocrystal against indentation. One may argue that a perfect crystal specimen can be made by ultra-fine polishing[20]. Unfortunately, it has not been the process of specimen preparation for nano-indentation.

Secondly, it is unclear how the microstructural change in a silicon monocrystal, such as amorphous transformation, influences its indentation properties. There have been many reports on the nano-indentation of both ceramics and silicon (e.g., Page, et al.,[14]

* Received 2nd October, 1998

** Department of Mechanical and Mechatronic Engineering, The University of Sydney, NSW 2006, Australia. E-mail:zhang@mech.eng.usyd.edu.au

NII-Electronic Library Service

Weppelmann, et al.,[16]). The load-displacement curves showed common features of "pop-in" and "pop-out". As the mechanisms of deformation of these materials under nano-indentation have not been fully understood, these experimental observations have led to controversial explanations. They have been considered as the result of microcracking, plastic deformation or phase transformation. Zhang and Mofid[18] showed that if the bifurcation of the loading curve in silicon indentation is elucidated by plastic deformation, von Mises yield criterion for metals can predict accurately the onset of 'plastic yielding' provided that an *equivalent yield stress* is used to replace the conventional yield stress in the von Mises function. However, the physical meaning of such a replacement is unclear and the "pop-out" during unloading cannot be explained. It was also found that the stresses in a silicon specimen during unloading do not suggest microcracking. By comparing with the critical hydrostatic stress for phase transformation (Hu, et al.,[21]), Weppelmann, Field and Swain[16] concluded that the phenomenon of "pop-out" was caused by amorphous phase transformation.

All the above studies did not consider the effect of surface roughness on nano-indentation. On the nanometre scale, as a matter of fact, surface asperities play a central role. For example, surface asperities always deform first before a full contact takes place between indenter and specimen. In the transient process, localised microstructural change may occur and alter the overall response of indentation. On the other hand, if the indenter and specimen surfaces are sufficiently smooth, the indentation will be influenced by surface energy, as pointed out by Johnson, Kendall and Roberts[22]. When surface roughness in comparable to or larger than the indentation scale, the surface energy effect becomes unmeasurable. In addition, probably because of the capacity of the load measurement devices in ordinary nano-indentation tests, unloading of indentation in all the above studies was considered to be complete when the load reduced to zero. This ignored the adhesion effect due to surface energy on the possible microstructural change that would in turn alter the mechanical properties of the specimen subjected to repeated loading. A thorough investigation into the mechanics and physics in silicon nano-indentation is therefore necessary.

The molecular dynamics analysis (MDA) has shown its unique advantage in studying the deformation of a solid on the nanometre and atomic scales and is particularly useful when a microstructural change during deformation becomes a major concern[11),(23)-(27)]. The application of the method to indentation of metals (e.g., Belak & Stowers[23], Hoover, et al.,[25]) showed that a great deal of details in the atomic lattice distortion of specimens can be revealed. Furthermore, an MDA deals with perfect crystal structure and perfectly smooth surfaces easily so that true deformation mechanisms of a silicon monocrystal under indentation can be explored.

With the aid of the molecular dynamics analysis, the present paper focuses on some fundamental problems of mechanics and physics associated with the nano-indentation of silicon monocrystals. To distinguish the mechanism of microstructural change, indentation is to be carried out in an absolute vacuum and clean environment.

Nomenclature

A : an imagined plane that divides a body into two parts, Ω_1 and Ω_2, see Fig. 5
a : radius of projection of the contact area on xoy plane, see Fig. 1.
a-Si : amorphous silicon
d : indentation depth, defined as the penetration of the top surface of an indenter into a silicon surface
E : Tersoff energy, defined by Eq.(1)
$\boldsymbol{F}$: resultant interatomic force through area S, see Eq.(4) and Fig. 5
$\boldsymbol{f}$: atomic interaction force during indentation
k : siffness
L : side length of the control volume, see Fig. 1
L_c : side length of a unit cell of silicon (=0.543 nm)
m : mass of an atom
N_A : number of atoms included in the imagined element for stress analysis
N_B : number of atoms in the volume outside the element below plane S
N_c : number of carbon-silicon atom pairs in contact
P : total indentation load
R : radius of a hemispherical diamond indenter
r : separation between two atoms, ie, length of bond
r_a : theoretical radius of an atom
S : base area of the imagined element, Γ, for stress analysis, see Fig. 5
T : period of vibration of an atom
V : indentation velocity
Γ : an imagined element in Ω_1 for stress analysis, see Fig. 5
$\boldsymbol{\sigma}$: stress vector, defined by Eq.(4); see also Fig. 5
τ : shear stress
θ_{ijk} : angle between atomic bonds ij and ik, see Fig. 2

NII-Electronic Library Service

Ω_1: the upper part of the body divided by plane A, see Fig. 5
Ω_2: the lower part of the body divided by plane A, see Fig. 5

Superscripts
oct: octahedral
max: maximum

Subscripts
c: critical
c-c: interaction between carbon-carbon atoms
c-si: interaction between carbon-silicon atoms
si-si: interaction between silicon atoms
i, j, k: atom i, j and k, respectively
x, y, z: x-, y- and z-direction, see Fig. 1

2. Theory

2.1 Modelling

The specimen of a silicon monocrystal and the diamond indenter are shown in Fig. 1. The initial temperature of the indentation system is 293°K. The hemispherical diamond indenter with radius R moving in z-direction with a constant speed V indents into the silicon on one of its (100) plane. The definition of indentation depth in the atomic analysis needs to be clarified specifically. In a conventional study of indentation, the indentation depth is the penetration of the indenter measured from the surface of the specimen. On the atomic scale, however, a definite surface does not exist because nucleuses are surrounded by electron clouds. To resolve this problem conveniently, assume that the surfaces of the indenter and specimen are defined by the envelopes at the theoretical radii of their surface atoms, respectively. In this way, the indentation depth, d, which is the penetration of the diamond surface into the silicon surface becomes consistent with the conventional definition.

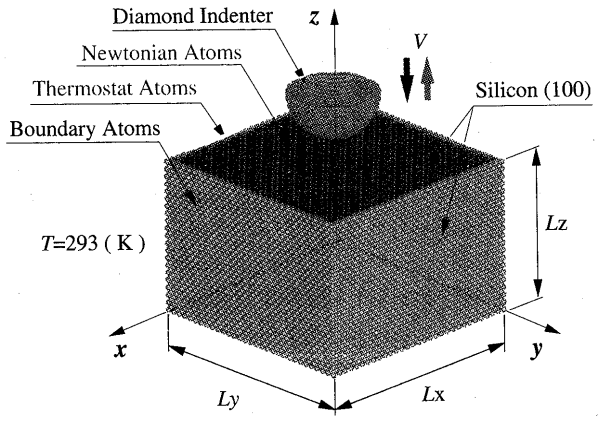

Fig. 1 The molecular dynamics model of nano-indentation of a silicon monocrystal. Note that the origin of the coordinate system is at the back-bottom corner of the specimen. The size of the control volume is determined by $L_x \times L_y \times L_z$. For all the analyses in this study, the initial temperature of the control volume is 293°K.

The dimension of the control volume (CV) of a silicon specimen must be sufficiently large to eliminate boundary effects. An error analysis showed that both the control volumes of $L_x \times L_y \times L_z = 6.5\,\text{nm} \times 10.3\,\text{nm} \times 10.3\,\text{nm}$ (i.e, 12 unit cells × 19 unit cells × 19 unit cells, containing 36 341 silicon atoms) and $10.8\,\text{nm} \times 16.3\,\text{nm} \times 16.3\,\text{nm}$ (i.e., 20 unit cells × 30 unit cells × 30 unit cells, containing 148 282 silicon atoms) are reliable, when the indentation dephth is of a few nanometres. They will be used in the present study accordingly, depending on the requirement of accuracy and efficiency.

To eliminate the rigid body motion of the specimen and guarantee a reasonable heat conduction outwards the CV, layers of boundary atoms, which are fixed to the space, and of thermostat atoms, which absorb the heat conducts towards the CV boundary, are arranged to surround the Newtonian atoms of silicon in the CV except its top (100) surface subjected to indentation, see Fig. 1.

2.2 Interatomic Potential

Silicon atoms are covalently bonded so that Tersoff potential[28] is used to describe the interactions between silicon atoms. As shown in Fig. 2, assume that j and k are the neighbouring atoms of atom i, that the atomic bond lengths of atoms i and j and of i and k are r_{ij} and r_{ik}, and that the angle between bonds ij and ik is θ_{ijk}. Then the total Tersoff energy, E, can be expressed as

$$E = \frac{1}{2}\sum_{i \neq j} W_{ij} \qquad (1)$$

where W_{ij} is the bond energy so that the summation in the equation is about all the atomic bonds in the control volume. W_{ij} is a function of repulsive pair potential, f_R, and attractive pair potential, f_A, and has the form of

$$W_{ij} = f_C(r_{ij})[f_R(r_{ij}) + b_{ij} f_A(r_{ij})], \qquad (2)$$

where

$$f_R(r_{ij}) = A_{ij} \exp(-\lambda_{ij} r_{ij}),$$
$$f_A(r_{ij}) = -B_{ij} \exp(-\mu_{ij} r_{ij})$$

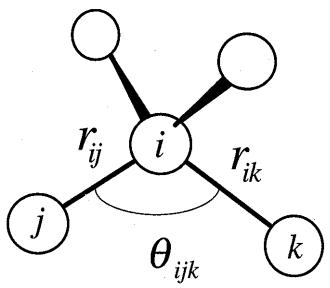

Fig. 2 Atomic bonds among silicon atoms

NII-Electronic Library Service

Table 1 Parameters in Tersoff potential for carbon and silicon[28),(29)]

	Carbon	Silicon
A (eV)	1.3936×10^{3}	1.8308×10^{3}
B (eV)	3.4670×10^{2}	4.7118×10^{2}
λ (nm^{-1})	34.879	24.799
μ (nm^{-1})	22.119	17.322
β	1.5724×10^{-7}	1.1000×10^{-6}
n	7.2751×10^{-1}	7.8734×10^{-1}
c	3.8049×10^{4}	1.0039×10^{5}
d	4.384×10^{0}	1.6217×10^{1}
h	-5.7058×10^{-1}	-5.9825×10^{-1}
R (nm)	0.18	0.27
S (nm)	0.21	0.30
$\chi_{C-C}=1.0$	$\chi_{Si-Si}=1.0$	$\chi_{C-Si}=0.9776$

$$f_C(r_{ij})=\begin{cases}1 & r_{ij}\le R_{ij}\\ \frac{1}{2}+\frac{1}{2}\cos\left(\frac{r_{ij}-R_{ij}}{S_{ij}-R_{ij}}\pi\right) & R_{ij}\le r_{ij}\le S_{ij}\\ 0 & r_{ij}\ge S_{ij}\end{cases}$$

$$b_{ij}=\chi_{ij}(1+\beta_i^{n_i}\zeta_{ij}^{n_i})^{-1/2n_i},\quad \zeta_{ij}=\sum_{k\neq i,j}f_C(r_{ik})g(\theta_{ijk})$$

$$g(\theta_{ijk})=1+\frac{c_i^2}{d_i^2}-\frac{c_i^2}{d_i^2+(h_i-\cos\theta_{ijk})^2} \qquad (3)$$

$$\lambda_{ij}=\frac{1}{2}(\lambda_i+\lambda_j)\quad \mu_{ij}=\frac{1}{2}(\mu_i+\mu_j)$$

$$A_{ij}=\sqrt{A_iA_j}\quad B_{ij}=\sqrt{B_iB_j}$$

$$R_{ij}=\sqrt{R_iR_j}\quad S_{ij}=\sqrt{S_iS_j}$$

Other parameters in Eq.(3), such as A, B, R, S, λ, χ and μ, as listed in Table 1, are Tersoff potential parameters, depending on individual materials. With Eqs.(1) and (2), the interaction forces between silicon atoms can be obtained by calculating the gradient of E[11),(26)]. For the interactions between silicon and diamond atoms, Morse potential, which has been shown elsewhere[11),(26)], is used.

2.3 Temperature Conversion

A very important factor in a successful molecular dynamics analysis is the reliable conversion between the kinetic energy and temperature of an atom. There are three models available[29)], *ie*, Dulong-Petit model, which takes into account the independent lattice vibration, Einstein model, which is based on the consideration of the single characteristic frequency, and Debye model, which involves a range of frequencies. A comparison with the experimental measurement given by Sinnott[30)], see Fig. 3, shows that in the temperature regime encountered in the present indentation Debye model is the best for silicon but Einstein model is the most suitable for diamond. Thus these models will be used correspondingly in the atomic heat conversions in the present study.

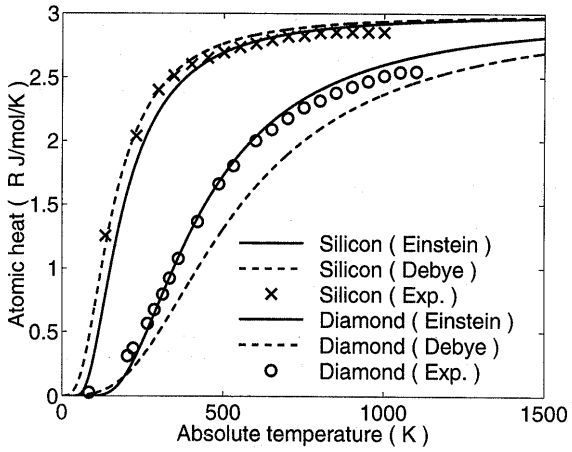

Fig. 3 A comparison of theoretical calculation of atomic heat with experimental measurement provided by Sinnott (28)

2.4 Time Step for Integration

Apart from the selection of interatomic potential and heat conversion, another critical issue in molecular dynamics analysis is an appropriate selection of time step for the numerical integration of the equations of motion of individual atoms. A too small step requires a huge computational cost but a too large step brings about unreliable results. Generally, a suitable time step should be less than at least 10 percent of the vibration period of an atom. Hence, the optimum time step is dependent on both the specific material and the potential function used.

With the Tersoff potential, an individual atom of silicon or diamond can be forced to move in a direction to show the corresponding stiffness, k, so that the period of vibration of the atom in the direction, T, can be determined by $T=2\pi(m/k)^{1/2}$, where m is the mass of the atom. The force-displacement relationships of a silicon and diamond atom in Fig. 4 then give rise to the average results listed in Table 2. A comparison between the molecular dynamics simulation using Tersoff potential and experimental measurement[30)] shows that a time step of 1.0 fs for diamond and 2.5 fs for silicon will provide sufficiently accurate integrations.

2.5 Stress Analysis

The concept of stress analysis needs to be developed to investigate the deformation of silicon on the atomic/nanometre scale, since silicon cannot be treated as a continuum on such a small scale and the conventional definition of stress is no longer valid. In addition, to understand the deformation purely induced by indentation, the effect of the natural interatomic forces in silicon before indentation must be eliminated.

Figure 5 shows a conceptual atomistic model for calculating stresses. Assume that a solid is divided

NII-Electronic Library Service

into an upper part, Ω_1, and a lower part, Ω_2, by a plane A. Consider a small element, Γ, in Ω_1 with a base area S in plane A. The stress vector on S is defined by

$$\sigma=\frac{F}{S} \tag{4}$$

where F is the resultant force on S induced by the interaction between the atoms in Ω_2 and those in Γ and should be calculated by

Table 2 Vibration period of diamond and silicon atoms and time steps for integration

	Diamond	Silicon
m ($\times 10^{-26}$ kg/atom)	1.9944	4.6636
$k=\left.\frac{d^2E}{dr^2}\right\|_{r=0}$ (N/m)	966.38 [100] 971.69 [111]	252.53 [100] 255.71 [111]
T (fs) [111]	28.46	84.85
Experiment (fs)	32.46	84.03
Time Step (fs)	1.0	2.5

$$F=\sum_{i=1}^{N_A}\sum_{j=1}^{N_B} f_{ij}-\sum_{i=1}^{N_A}\sum_{j=1}^{N_B} f_{oij} \tag{5}$$

in which N_A is the number of atoms in Γ, N_B is the number of atoms in Ω_2 and f_{ij} and f_{oij} are the interatomic force vectors during and before indentation, between atom i in Γ and atom j in Ω_2. It is important to note that in continuum mechanics a stress vector is defined at a methematical point but in the definition here on the atomic scale area S should always be finite. Moreover, to obtain a representative stress vector on S, the height of Γ must be selected in a way that the interaction force between atom j in Ω_2 and atom i in Ω_1 but beyond the top surface of Γ is negligible. In the present stress analysis, it is found that the optimum size for element Γ is $2L_c\times 2L_c\times L_c$, as shown in Fig. 5, where $L_c=0.543$ nm is the side length of a unit cell of silicon.

2.6 Contact Area

There are two ways to calculate the contact area between an indenter and specimen on the nanometre scale. One is to take count of the number of C-Si

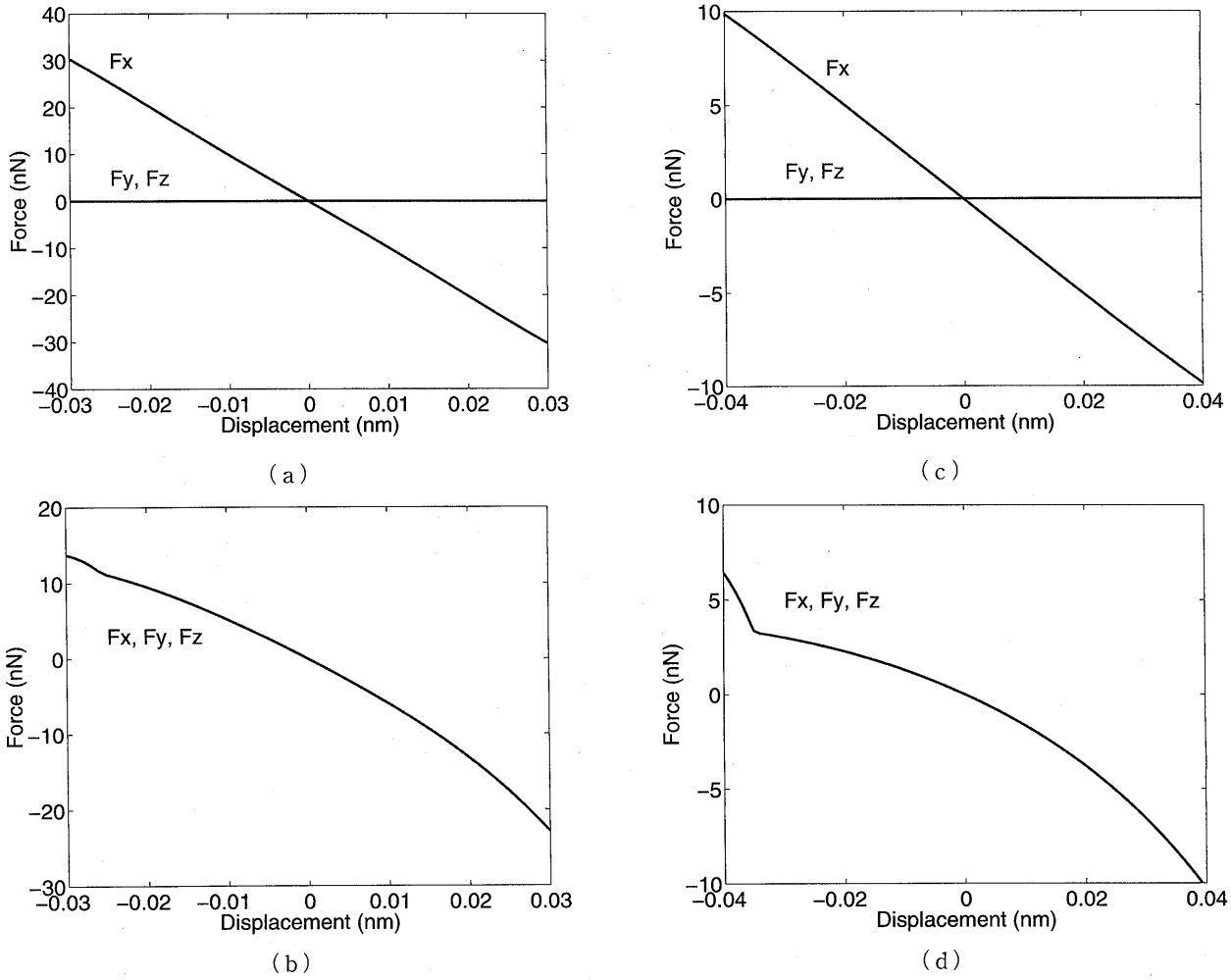

Fig. 4 Force-displacement relationship when moving an atom in a particular direction. (a) moving a silicon atom in x-direction ([100]), (b) moving a silicon atom in the octahedral direction ([111]), (c) moving a diamond in x-direction ([100]), (d) moving a diamond in octahedral direction ([111])

NII-Electronic Library Service

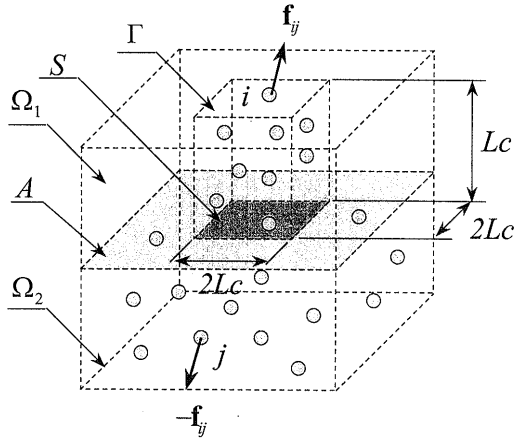

Fig. 5 Concept of stress vector on the atomic scale

atom pairs in contact and then add up the atomic contact areas. In this way, if the theoretical radius of an atom is r_a and the number of atom pairs in contact is N_c, the total contact area is

$$A^c_{\text{atomic}}=\pi r_a^2 N_c \qquad (6)$$

The other method is to follow the conventional approach in a continuous model. In this case, one needs to determine first the outer profile of the contact zone, take an average radius, R_a*1, of the contact zone projection on xoy plane and then compute the spherical contact area by

$$A^c_{\text{cont}}=2\pi R^2\left(1-\sqrt{1-\frac{R_a^2}{R^2}}\right) \qquad (7)$$

where subscript "cont." indicates continuous. In so doing, it has assumed that the whole area within the border of the contact zone is in continuous contact.

3. Results and Discussion

3.1 Deformation Characteristics

A complete load-displacement curve of indentation, as shown in Fig. 6(a), consists of the loading path, ABCDEFG, and the unloading path, GHIJKLM. The significant deviation between loading and unloading paths indicates that a remarkable inelastic deformation occurs during indentation. Compared with any experimental measurements of nano-indentation (e.g., those presented by Weppelmann, et al.,[16]), the present curve shows two distinguished features demonstrated by part ABC in the loading path and part IJKLM in the unloading path. From state A to C, the indentation load is negative (tensile), which means that when the diamond indenter approaches to the silicon specimen the surface atoms in silicon and diamond first experience attractive forces before compression. Thus even under a large tensile indentation load, as shown in Fig. 6(b), the contact area between the indenter and specimen is finite. However, at the end of loading (state G in Fig. 6(a)), the contact area becomes very large. Thus at the state with zero indentation load during unloading (state I in Fig. 6(a)), the contact area is still large, due to the attraction between silicon and diamond atoms. The attraction keeps increasing until state L although the contact area is continuously shrinking (Fig. 6(b)). Such process of contact area shrinkage can be more clearly seen in Figs. 6(c) and 6(d) through a cross-sectional view of the atomic lattice deformation.

Under static and purely elastic conditions, Johnson, Kendall and Roberts[22] developed the well known JKR theory to modify the Hertzian prediction of contact area by considering the effect of surface adhesion energy. For the present indentation configuration, the JKR theory gives rise to

$$\left\{\frac{P}{P_c}-\left(\frac{a}{a_c}\right)^3\right\}^2=4\left(\frac{a}{a_c}\right)^3 \qquad (7)$$

and indicates that contact breaks when $P=-5P_c/9$ at $a=a_c/3^{2/3}$, where P_c is the maximum tensile indentation load and a_c is the corresponding contact area. Figure 7 compares the prediction from Eq.(7) and the result from molecular dynamics simulation, where P_c and a_c are taken as the indentation loads and contact areas at states B and L, respectively, for loading and unloading. It is interesting to note that in the vicinity of $P=-P_c$, the predictions of the JKR theory are in good agreement with the present results, although the theory is only valid for an elastic and static indentation while significant inelastic deformation occurred in the present cases and indentation speed varied largely from 20 m/s to 200 m/s. This is because the JKR theory gives an identical result at $P=-P_c$. Thus when a/a_c changes not so sharply with P/P_c, the prediction from the JKR theory and molecular dynamics analysis should not be remarkably different. Thus in a sense, JKR theory can also be used to calculate the contact area in the vicinity of $P=-P_c$, although the origin of deformation has been different.

Under purely elastic indentation, the contact will become unstable when P reaches $-5P_c/9$ during unloading, as pointed out by Johnson, Kendall and Roberts[22]. In an inelastic indentation, however, the occurrence of such contact instability depends on the strength of atomic interaction of the material subjected to indentation and that between the material and the indenter. In all the indentation tests in this study, the instability of contact during unloading never happens, as shown in Fig. 7. When indenting some other

*1 As the deformation of silicon is anisotropic, the border of the contact area is not exactly a circle. However, as will be shown later in this paper, the anisotropy is not significant. For convenience, assume that the contact zone is within a circle with an average radius R_a.

NII-Electronic Library Service

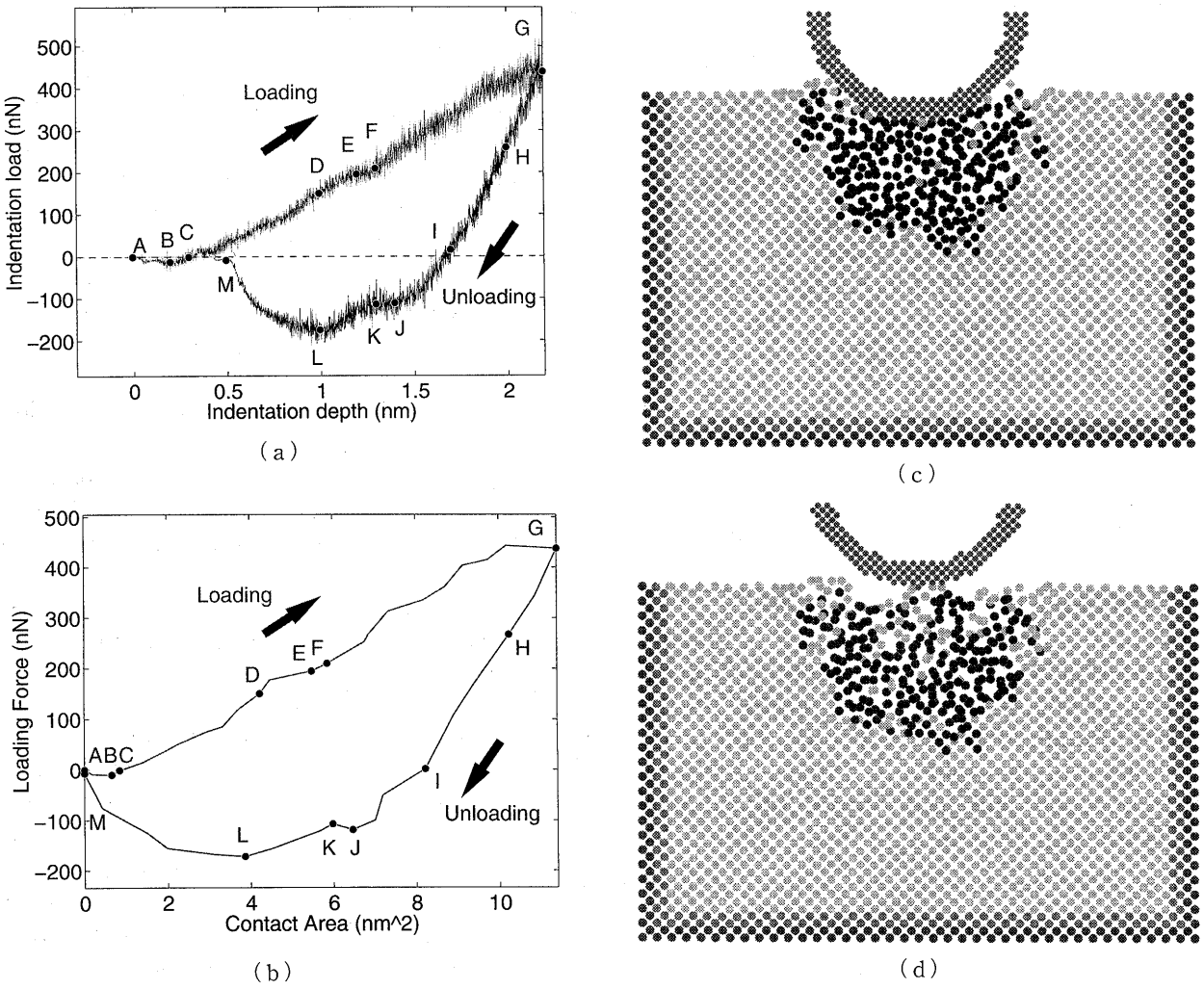

Fig. 6 Overall response of silicon nano-indentation in a complete loading-unloading cycle. The indentation conditions are: $d^{max}=2.194\,7$ nm and $R=2.1$ nm. The diamond indenter in this case contains 1 818 atoms. (a) load-displacement curve ($V=40$ m/s), (b) load-contact area curve ($V=40$ m/s), (c) contact during unloading at $P=-128$ nN ($V=200$ m/s, $d=0.694\,7$ nm), (d) contact during unloading at $P=-16.4$ nN ($V=200$ m/s, $d=0.194\,7$ nm). In (c) and (d), compare the difference of adhesion between the diamond and silicon surfaces

materials, as reported by Durig and Stalder[31] for instance, instability still occurs although significant plastic deformation appears.

3.2 Microstructural Change

In the whole indentation process, dislocations do not appear. Inelastic deformation is solely caused by amorphous phase transformation*2, as shown in Fig. 8. In other words, inelastic deformation in silicon under nano-indentation is due to the viscous flow in the amorphous zone rather than other mechanisms such as plasticity induced by dislocations. Viscous flow via amorphous change in this case needs much less deformation energy. The above conclusion supports strongly the recent experimental findings in the ultra-fine grinding and polishing of silicon monocrystals[8],[19],[20] that amorphous layer always exists*3 but dislocations do not appear until the depth of abrasive penetration reaches a critical value.

Amorphous silicon appears shortly after indentation begins, see Fig. 8(a). In the initial stage such a phase transformation localizes in a few layers of silicon atoms that are under the indenter. It means that the purely elastic deformation takes place only in a very narrow range. When indentation proceeds to a certain level, say state D for the case in Fig. 6(a), amorphous growth becomes much faster. From D to F, the number of amorphous atoms increases by 218%

*2 Each atom in the crystal structure of silicon has four first neighbour atoms. Thus if the number of the first neighbour atoms of an atom is larger than 4 and the position of the atom does not follow the crystal lattice, this atom becomes an amorphous atom.

*3 Only under some special polishing conditions, both amorphous zone and dislocations disappear. Details can be found in Refs.(8), (19), (20).

NII-Electronic Library Service

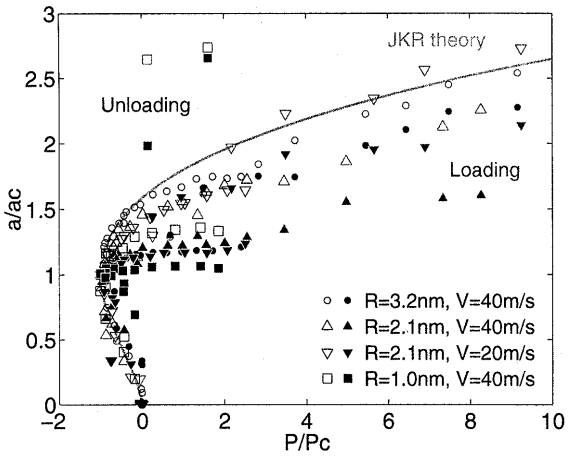

Fig. 7 A comparison with the JKR theory. The hollow marks are the projections of A^c_{atomic} on xoy plane calculated by Eq.(6) and the solid ones are those of A^c_{cont} calculated by Eq.(7). The contact areas during loading and unloading are different and are distinguished by different colours.

and the volume of amorphous zone increases by 202%, see Figs. 9(a) and 9(b). The fast phase change from D to F causes a rapid temperature rise (Fig. 9(c)). Since amorphous silicon is much softer than the crystal silicon, the fast amorphous growth introduces a local softening phenomenon from E to F. On the load-displacement curve of indentation (Fig. 6(a)), the softening brings about a clear slope change from DCE to EF. As a result, the amorphous phase is condensed quickly so that the density of the phase increases considerably from D to F, see Fig. 9(d). After state F, the variation of all the above (amorphous growth, temperature rise, contact area development and denstity increment of the amorphous phase) becomes steady and linear. Thus from F to G, both the elastic deformation in the crystal zone (bending of atomic lattice) and the further development of amorphous phase have linear contributions to the overall deformation and gives rise to a linear load-displacement relationship from F to G, as shown in Fig. 6(a). In this stage, the elastic deformation zone becomes much larger (Figs. 8(b) to 8(d)) and the average relative density of the amorphous phase increases from 1.55 to 1.70 (Fig. 9(d)).

During unloading, the deformation behaviour from G to I is mainly the result of elastic recovery of the crystal lattice, although certain amount of re-crystallisation, i.e., a reverse phase change from amorphous to crystal, happens, as shown in Figs. 8(d) to 8(e). This phenomenon is more evident at the very begining of unloading from G to H. In this period, the total volume of the amorphous zone decreases linearly by 18.2% (Fig. 9(b)), the total number of amorphous atoms reduces by 14.8% (Fig. 9(a)) but the average

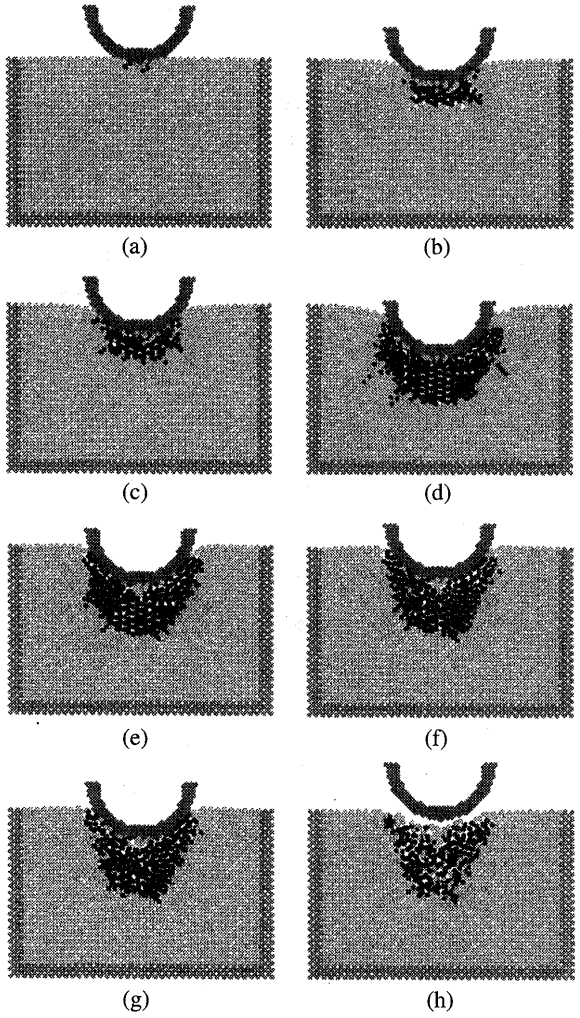

Fig. 8 Amorphous development and elastic deformation in silicon. Note the obvious elastic bond bending from (b) to (d) during loading and the elastic recovery from (d) to (e) during unloading. A re-crystallisation can be clearly observed by comparing the shrinkage of the amorphous zone from (e) to (h). Indentation conditions are: $d^{\max}$= 2.194 7 nm, R=2.1 nm and V=40 m/s. Refer the deformation states marked in Fig. 6(a).(a) at state C (d=0.294 7 nm), (b) at state D (d=1.094 7 nm), (c) at state E (d=1.294 7 nm), (d) at state G (d=2.194 7 nm), (e) at state I (d=1.694 7 nm), (f) at state J (d=1.394 7 nm), (g) at state K (d= 1.294 7 nm), (h) at state M (d=0.494 7 nm).

density of amorphous phase increases by 1.2% (Fig. 9(d)). This means that the deformation is dominated by elastic recovery so that the load-displacement curve behaves also linearly. It is interesting to note that the contact area (Fig. 6(b)) and temperature of the specimen (Fig. 9(c)) also decreases linearly. After state I, the effect of elastic recovery is no longer dominant. The continuous re-crystallisation and density change with almost a constant amorphous volume make the load-displacement curve vary in a

NII-Electronic Library Service

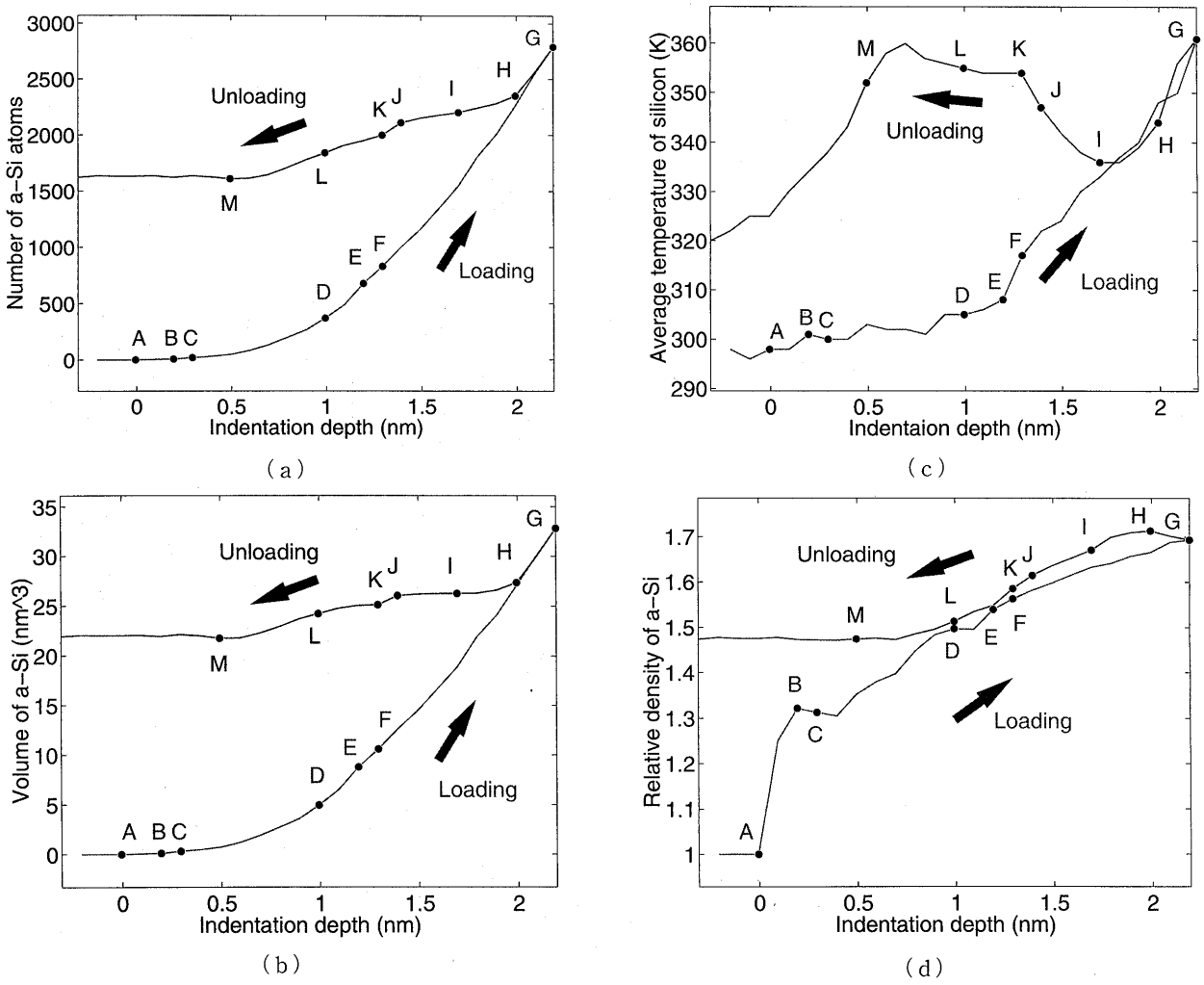

Fig. 9 Variation of key quantities during indentation. Indentation conditions are: $d^{max}=2.194\,7$ nm, $R=2.1$ nm and $V=40$ m/s. (a) number of amorphous silicon, (b) volume of amorphous zone, (c) average temperature rise in the specimen, (d) the ratio of the average density of amorphous silicon to the density of crystal silicon. The notation a-Si means amorphous silicon.

complex manner from I to M. Because of this, temperature rises again. From J to K, re-crystallisation becomes dominant, leading to a fast decrease of density, a drop of amorphous volume and a weaker interaction with the diamond indenter. This makes the load-displacement curve bend from J to K. The re-crystallisation process finishes shortly after state L when the number of amorphous atoms becomes constant, as shown in Fig. 9(a). It is also clear that state L is critical beyond which the indenter-specimen contact becomes purely adhesive since both the volume and density of amorphous zone become constant. After L, contact area shrinks quickly and finally vanishes at M with an residual indentation depth. An irreversible indentation mark thus remains due to the local density change of silicon, see Fig. 8(h).

A silicon monocrystal is anisotropic as its atomic structure implies. The anisotropy can be understood more directly by monitoring the development of the amorphous zone. Figure 10 shows the profile change of the amorphous zone in xoy plane (see Fig. 1) when observing in the positive z direction. Clearly, amorphous phase grows with different rates in different directions and the difference becomes greater when indentation proceeds. However, during unloading re-crystallisation also occurs with different rates in different directions. As shown in Fig. 11, in the direction that amorphous phase grows faster during loading re-crystallisation also goes faster during unloading. As a result, the amorphous zone during and after unloading becomes quite axisymmetric. Nevertheless the deformation anisotropy is not remarkable in the whole loading and unloading process. Indeed, the anisotropy ratio of a silicon monocrystal under pure elastic deformation is 0.64, which deviates from an ideally isotropic material by only 36%[32].

NII-Electronic Library Service

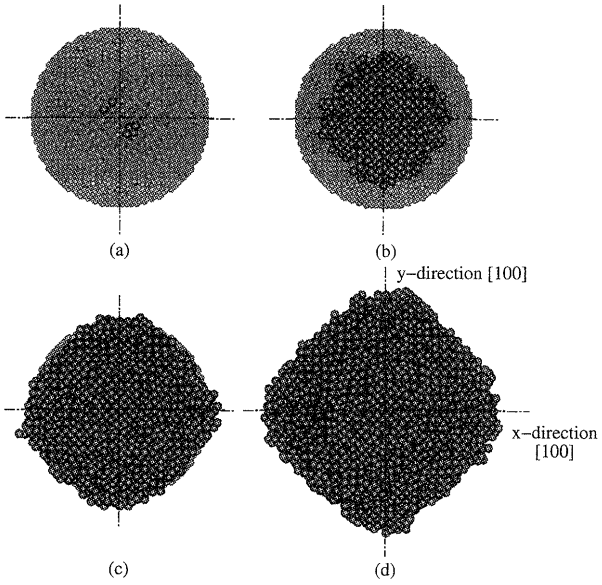

Fig. 10 A bottom view of the development of amorphous zone during loading process when indentation depth d increases. The blue balls are diamond atoms and brown ones are amorphous silicon atoms. Indentation conditions are: $d^{max}=3.194\,7$ nm, $R=3.2$ nm and $V=40$ m/s. The indenter in this case contains 4 533 diamond atoms. (a) $d=0.194\,7$ nm, (b) $d=1.194\,7$ nm, (c) $d=2.194\,7$ nm, (d) $d=3.194\,7$ nm

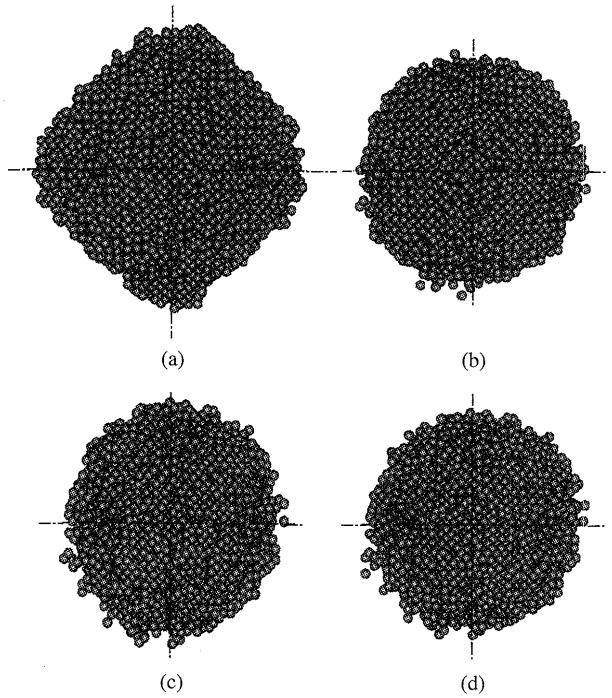

Fig. 11 A bottom view of the development of amorphous zone during unloading. The blue balls are diamond atoms and brown ones are amorphous silicon atoms. Indentation conditions are: $d^{max}=3.0$ nm, $R=3.2$ nm and $V=40$ m/s. (a) $d=3.194\,7$ nm, (b) $d=2.194\,7$ nm, (c) $d=1.194\,7$ nm, (d) after complete unloading

3.3 Stress Criteria for the Onset of Inelastic Deformation

The above discussion on the atomic lattice deformation of silicon shows the physics of microstructural change in silicon indentation. A natural question is how to conveniently predict the onset of such inelastic deformation. This, like the criteria for initial yielding of metals, is of primary importance to a proper design, fabrication and application of a silicon component.

The above discussion has shown that amorphous phase transformation from the initial crystal structure is due to the severe atomic lattice distortion, which breaks the original atomic bonding among silicon atoms. Thus the onset of such inelastic deformation must have a close relationship with the distortion energy. On the other hand, to break the atomic bonds in a perfect monocrystal of silicon, one must apply a sufficiently large shear stress that is close to the theoretical shear stress of silicon. Since the distortion energy in a deformable body is proportional to the octahedral shear stress (OSS), it is reasonable to examine the relationship of OSS with the inelastic deformation caused by amorphous change.

Using the method of stress calculation presented in Section 2 of this paper, the OSS in silicon can be examined over the whole control volume. This immediately leads to the conclusion that an amorphous phase transformation occurs in the crystal silicon when the OSS reaches a critical value, τ_c^{oct}, which is 4.6 GPa in direction [100] and 7.6 GPa in direction [110] and is close to the theoretical shears stress of 9.23 GPa($=G/2\pi$). Any direction between them must have $4.6\,\text{GPa}<\tau_c^{oct}<7.6\,\text{GPa}$, as shown in Fig. 12. The above τ_c^{oct} is in agreement with that found in contact sliding[27], cutting, grinding and polishing[19] and indentation[34]. Therefore the present octahedral shear stress criterion and the threshold τ_c^{oct} given above can be used to predict the initiation of amorphous change in silicon in the processes of indentation, sliding and ultra-precision machining such as nano-cutting, nano-grinding and nano-polishing, when carrying out a microscopic or macroscopic analysis. On the other hand, as illustrated in Figs. 10 and 11, the deformation anisotropy in crystal silicon is not so significant and in addition the amorphous silicon has a random structure. Thus the deformation can be viewed approximately as an isotropic process when a large number of atoms are involved. With such a consideration, an average threshold of $\tau_c^{oct}=6.1$ GPa can be used to predict the onset of inelastic deformation in silicon monocrystals due to amorphous phase transformation. To have a more accurate prediction, however, a more comprehensive criterion that can reflect the effect of anisotropy must be developed.

NII-Electronic Library Service

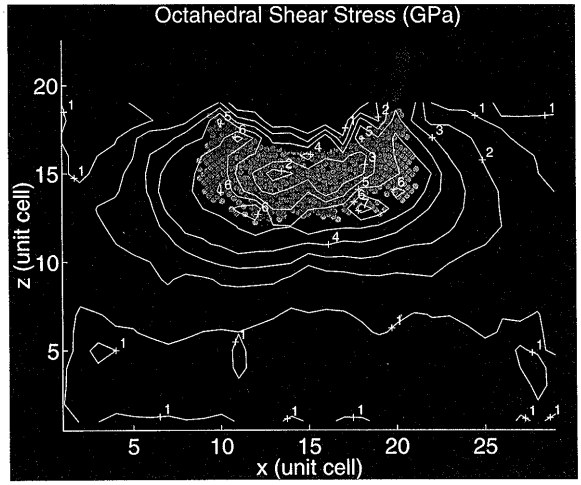

(a)

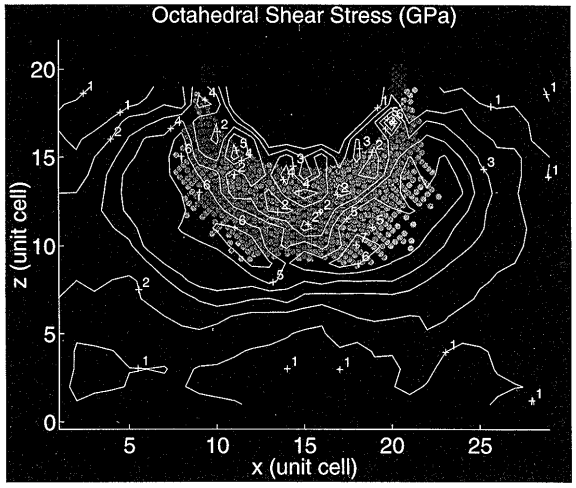

(b)

Fig. 12 A comparison of predictions of stress criterion with molecular dynamics analysis. The blue balls are diamond atoms and red ones are amorphous silicon atoms. The yellow curves indicate octahedral shear stesses. It is clear to see here that the threshold for the onset of amorphous change is 4.6 GPa $< \tau_c^{oct} = 5.5$ GPa < 7.6 GPa. Indentation conditions are $R=3.2$ nm and $V=40$ m/s. (a) $d=2.194\,7$ nm, (b) $d=3.194\,7$ nm

The octahedral shear stress criterion is similar to the von Mises criterion for an initial plastic yielding of a metal except that the von Mises criterion used the initial yield stress of the metal under a simple tension. Because of the similarity, one may immediately think that Tresca criterion for metal yielding may also lead to a good prediction since the physical difference between von Mises and Tresca criteria is that the former concerns the critical value of OSS and the latter considers the maximum shear stress (MSS). A test shows that the lotus of MSS also fits well the boundary of amorphous transformation in the present indentation provided that a critical value of $\tau_c^{max}=5.3$ GPa in direction [100] and 10.3 GPa in direction [110] is used. For metals, τ_c^{max} and τ_c^{oct} have a simple relationship that can be determined by performing a simple tensile and a pure shearing test. For the present phase transformation in silicon, however, their relationship is unclear, because phase transformation may not happen under those simple stress states. Further studies are thus necessary.

Used the experimental observations of Hu, et al.,[21] under pure hydrostatic conditions that are different from indentation, Pharr, et al.,[33] tried to explain the formation mechanism of amorphous change in nano-indentation. They concluded that the hydrostatic stress component was the key factor and deviatoric stresses were less important to phase transformation. They thought that amorphous change occurred when the indentation load generated a sufficiently high hydrostatic stress component. Weppelmann, et al.,[16] also concluded that the hydrostatic stress component at the onset of transformation during loading was 11.3 GPa and at the reverse transformation during unloading was 8.4 GPa, which were almost identical with the values measured by Hu, et al. (11.3 to 12.5 GPa during hydrostatic loading and 8.5 to 10.8 GPa during hydrostatic unloading). However, these conclusions were based on the maximum hydrostatic stress generated at a given indentation load. They overlooked the difference between the onset of amorphous phase and the development of an existing amorphous zone and ignored the dependence of such inelastic deformation on loading history. For example, if the hydrostatic stress, with the threshold of 11.3 GPa, is used to measure the initiation of phase change during loading, it can be seen easily from Figs. 12 and 13 that the predicted amorphous zone will be much smaller than it should be. An error will also occur during unloading if the hydrostatic stress criterion with the threshold of 8.5 GPa is applied. It is therefore clear that hydrostatic stress cannot be used to predict the onset of amorphous change in indentation.

Although amorphous phase transformation in silicon can be introduced by either a pure hydrostatic stress or an indentation, the mechanism is different. This can be understood more easily in the following way. One can imagine that phase transformation will not happen in an atomically isotropic material subjected to a hydrostatic pressure, because in such an idealised case increasing the pressure only changes the atomic distance uniformly but not the atomic lattice structure of the material. However, as the atomic lattice of monocrystalline silicon is anisotropic, a hydrostatic pressure will introduce internal lattice distortion in the material and if it is great enough will lead to a change of atomic structure and thus a phase transformation. Indentation introduces significant

NII-Electronic Library Service

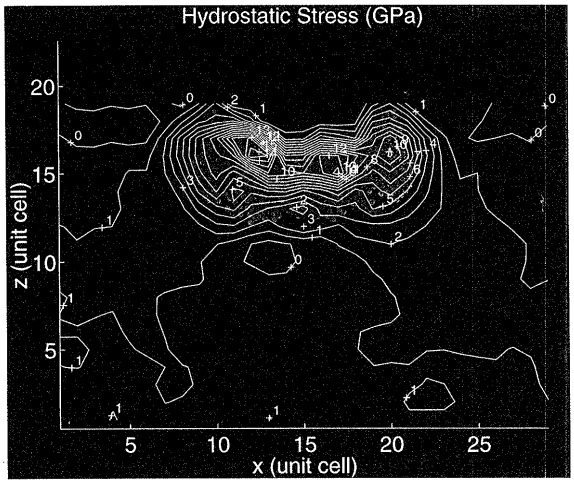

(a)

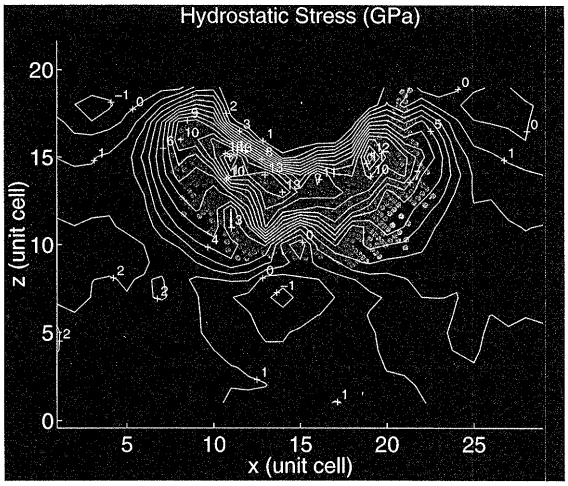

(b)

Fig. 13 Hydrostatic stress and deformation in silicon during loading. Indentation conditions are R=3.2 nm and V=40 m/s. (a) d=2.194 7 nm, (b) d=3.194 7 nm

shearing stresses, which breaks atomic bonds more easily than in the case under a pure hydrostatic stress. This makes the initiation of amorphous phase easier. However, hydrostatic stress will affect greatly the further development of amorphous phase after its initiation by shear stresses. This is shown indirectly by Fig. 9(d), where we can see that the density of a-Si increases significantly, indicating that there is a large volume change. It then follows from the above discussion that a critical shearing stress initiates the amorphous phase transformation, but after the critical moment of the initiation, hydrostatic stress plays an important role in driving the further transformation development.

From the above discussion, it also becomes clear why Zhang and Mahdi[18] could predict the 'onset of plastic deformation' during loading when using the equivalent yield stress to replace the conventional yield stress in the von Mises function. Their equivalent yield stress is proportional to the present threshold of amorphous phase transformation via shear on the octahedral plane, τ_c^{oct}. However, in the finite element analysis, the effects of the rapid density increase and temperature-dependent properties of the amorphous phase were excluded. As can be seen now, these effects play a significant role in determining the overall load-displacement behaviour in nano-indentation.

3.4 Effects of Indentation Speed and Radius of Indenter

The deformation mechanism of silicon does not change when indentation speed varies from 4 m/s to 200 m/s or when the radius of indenter changes from 1 nm to 3.2 nm. In other words, with different indentation speeds or radii of indenter, the process of phase transformation, variation of volume and density of amorphous zone, characteristics of load-displacement curves, variation of contact area and change of temperature all follow the same rules as discussed in the previous sections. In general a smaller indentation speed or a smaller radius of indenter leads to a smaller amorphous zone, a lower temperature rise, a smaller contact area and indentation load. However, it is interesting to note that when the maximum indentation strain d^{max}/R is less than unity, the average slope, $\partial P/\partial d$, from state C to G and that from G to I, as shown in Fig. 6(a), are almost unchanged, although both the radius of indenter and speed of indentation vary. It is a general fact that increasing the indentation speed raises the indentation load at a given depth of indentation and hence $\partial P/\partial d$ must change. However, the insensitivity to indentation speed observed here is understandable if one notes that the temperature rise at a higher indentation speed increases the viscous fluidity of the amorphous phase and thus compensates the dynamic effect to a great extent*4.

If the maximum indentation strain d^{max}/R exceeds unity, the amorphous zone is larger than the diameter of indenter. In this case, viscous flow of amorphous silicon aside the indenter occurs and hence the resistance of the specimen to indentation drops significantly, as shown in Fig. 14.

4. Conclusions

A detailed molecular dynamics analysis of nano-indentation of silicon monocrystals by diamond using the Tersoff potential function in conjunction with Debye and Einstein temperature conversions has been carried out successfully. New concepts of stress and contact area analyses have been developed. Through

*4 For example, the maximum specimen temperature with V=20 m/s is 361°K but that with V=200 m/s is nearly 450°K.

NII-Electronic Library Service

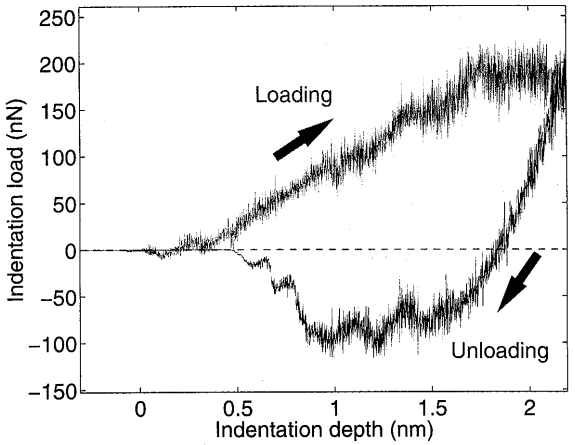

Fig. 14 Load-displacement curve in a complete loading-unloading cycle when d^{max}/R is larger than unity. Indentation conditions are $R=1.0$ nm, $d^{max}=2.194\,7$ nm and $V=40$ m/s. In this case, the indenter contains 394 diamond atoms.

a careful discussion, the following understanding of the mechanics and physics in silicon indentation has been gained.

(1) Amorphous phase transformation is the only cause of inelastic deformation. The size of the amorphous zone decreases during unloading because of the continuous re-crystallisation.

(2) The inelastic deformation due to phase change can be predicted by a criterion using either octahedral shear stress or maximum shear stress. However, the relationship between the thresholds τ_c^{oct} and τ_c^{max} is unclear and needs a further investigation.

(3) A hydrostatic stress can introduce amorphous change but in indentation it is the critical shearing stress that initiates the amorphous phase transformation. After the critical moment of the initiation, hydrostatic stress plays an important role in driving the further transformation development.

(4) The threshold values obtained here, $\tau_c^{oct}=4.6$ GPa and $\tau_c^{max}=5.3$ GPa in direction [100] and $\tau_c^{oct}=7.6$ GPa and $\tau_c^{max}=10.3$ GPa in direction [110], can be used for other microscopic and macroscopic analyses of the inelastic deformation of silicon monocrystals. To have an accurate prediction, a comprehensive criterion that can reflect the effect of anisotropy must be developed.

(5) The variation of the contact area between indenter and silicon follows a complex rule. However, the JKR theory can still be used for a rough estimation in the vicinity of $P=-P_c$ although the origin of deformation is different.

(6) The effect of changes of indenter radius and indentation speed is negligible when the maximum indentation strain is less than unity.

Acknowledgment

The continuous support from Australian Research Council to this work through its ARC Large Grant Scheme is very much appreciated. The first author thanks the helpful discussion with Prof KL Johnson of Cambridge University. Dr Nicole Bordes in the VisLab of Sydney University helped in the visualisation of the results.

References

(1) Johnson, K.L., Contact Mechanics, (1985), Cambridge University Press, Cambridge.
(2) Bolse, W. and Peteves, S.D., Indentation Characterisation of Silicon Nitride, J Testing & Evaluation, Vol. 23 (1995), p. 27-32.
(3) Lawn, B.R., Fracture of Brittle Solids, 2nd edition, (1993), Cambridge University Press, Cambridge.
(4) Milman, Y.V., Galanov, B.A. and Chugunova, S.I., Plasticity Characteristic Obtained through Hardness Measurement, Acta Metall. Mater., Vol. 41 (1993), p. 2523-2532.
(5) Pharr, G.M., Oliver, W.C. and Brotzen, F.R., On the Generality of the Relationship Among Contact Stiffness, Contact Area and Elastic Modulus during Indentation, J Mater. Res., Vol. 7 (1992), p. 613-617.
(6) Sakai, M., Energy Principle of the Indentation-Induced Inelastic Surface Deformation and Hardness of Brittle Materials, Acta Metall. Mater., Vol. 41 (1993), p. 1751-1758.
(7) Sharp, S.J., Ashby, M.F. and Fleck, N.A., Material Response under Static and Sliding Indentation Loads, Acta Metall. Mater., Vol. 41 (1993), p. 685-682.
(8) Zhang, L.C. and Yasunaga, N., (eds) Advances in Abrasive Technology, (1997), World Scientific, Singapore.
(9) Bhushan, B.(ed), Handbook of Micro/Nanotribology, (1995), CRC Press, Boca Raton.
(10) Persson, B.N.J., Sliding Friction: Physical Principles and Applications, (1998), Springer-Verlag, Berlin.
(11) Zhang, L.C. and Tanaka, H., Towards a Deeper Understanding of Friction and Wear on the Atomic Scale: A Molecular Dynamics Analysis, Wear, Vol. 211 (1997a), p. 44-53.
(12) Callahan, D.L. and Morris, J.C., The Extent of Phase Transformation in Silicon Hardness Indentations, J Mater. Res., Vol. 7 (1992), p. 1614-1617.
(13) Hainsworth, S.V. and Page, T.F., Nanoindentation Studies of the Chemomechanical Effect in Sapphire, J Mater. Sci., Vol. 29 (1994), p. 5529-5540.
(14) Page, T.F., Oliver, W.C. and McHargue, C.J., The Deformation Behaviour of Ceramic Crystals Subjected to Very Low Load (Nano) Indentations, J Mater. Res., Vol. 7 (1992), p. 450-473.
(15) Sadeghipour, K., Chen, W. and Baran, G., Spheri-

NII-Electronic Library Service

cal Micro-Indentation Process of Polymer-Based Materials: A Finite Element Study, J. Phys. D: Appl. Phys., Vol. 27 (1994), p. 1300-1310.
(16) Weppelmann, E.R., Field, J.S. and Swain, M.V., Observation, Analysis and Simulation of the Hysteresis of Silicon Using Ultra-Micro-Indentation with Spherical Indenters, J Mater. Res. Vol. 8 (1993), p. 830-840.
(17) Yokohata, T. and Kato, K., Mechanism of Nanoscale Indentation, Wear, Vol. 168 (1993), p. 109-114.
(18) Zhang, L.C. and Mahdi, M., The Plastic Behaviour of Silicon Subjected to Micro-Indentation, J Mater. Sci., Vol. 31 (1996), p. 5671-5676.
(19) Zhang, L.C., Tanaka, H. and Zarudi, I., The Mechanism of Material Removal in Grinding and Polishing Silicon Mono-Crystals on the Nanometre Scale, In Proceedings of the 12th ASPE Annual Conference, ed. American Society of Precision Engineering, (1997), p. 462-465, American Society of Precision Engineering, Raleigh.
(20) Zarudi, I. and Zhang, L.C., Subsurface Damage in Single-Crystal Silicon due to Grinding and Polishing, J Materials Science Letters, Vol. 15 (1996), p. 586-587.
(21) Hu, J.Z., Merkle, L.D., Menoni, C.S. and Spain, I. L., Crystal Data for High-Pressure Phases of Silicon, Physical Review, B34 (1986), p. 4679-4684.
(22) Johnson, K.L., Kendall, K. and Roberts, A.D., Surface Energy and Contact of Elastic Solids, Proc R Soc London, A324 (1971), p. 301-313.
(23) Belak, J. and Stowers, I.F., The Indentation and Scraping of a Metal Surface : A Molecular Dynamics Study, In Proceedings of the NATO Advanced Study Institute on Fundamentals of Friction, ed. Singer, I.L. and Pollock, H.M., (1992), p. 511-520, Kluwer Academic Publishers, Dordrecht.
(24) Boercker, D.B., Belak, J., Stowers, I.F., Donaldson, R.R. and Siekhaus, W.J., Simulation of Diamond Turning of Silicon Surfaces, In Proceedings of the 7th Annual Meeting of American Society of Precision Engineering, ed. American Society of Precision Engineering, (1992), p. 45-48, American Society of Precision Engineering, Raleigh.
(25) Hoover, W.G., De Groot, A.J., Hoover, C.G., Stowers, I.F., Kawai, T., Holian, B.L., Boku, T., Ihara, S. and Belak, J., Large-Scale Elastic-Plastic Indentation Simulations via Nonequilibrium Molecular Dynamics, Physical Review, A42, (1990), p. 5844-5853.
(26) Tanaka, H. and Zhang, L.C., A Three-Dimensional Molecular Dynamics Modelling of Nano-Cutting Processes, In Proceedings of the Third International Conference on Progress in Cutting and Grinding, ed. Narutaki, N., Chen, D., Yamane, Y. and Ochi, A., (1994), p. 262-266, Japan Society of Precision Engineering, Osaka.
(27) Zhang, L.C. and Tanaka, H., Atomic Scale Deformation in Silicon Monocrystals Induced by Two-Body and Three-Body Contact Sliding, Tribology International, 31 (1998), p. 425-433.
(28) Tersoff, J., Modeling Solid-State Chemistry: Interatomic Potential for Multicomponent Systems, Physical Review, B39 (1989), p. 5566-5568.
(29) Kittel, C., Introduction to Solid State Physics, 7th edition, (1996), John Wiley & Sons, Inc., New York.
(30) Sinnott, M.J., The Solid State Physics for Engineers, (1958), p. 291, John Wiley & Sons, Inc., New York.
(31) Durig, U. and Stalder, A., In Physics of Sliding Friction, ed. Persson, B.N.J. and Tosatti, E., (1996), Kluwer, Dordrecht.
(32) Courthey, T.H., Mechanical Behaviour of Materials, (1990), p. 59, McGraw-Hill, Singapore.
(33) Pharr, G.M., Oliver, W.C. and Harding, D.S., J. Mater. Res, Vol. 6 (1991), p. 1129-1130.
(34) Zarudi, I. and Zhang, L.C., An Experimental Investigation into the Microstructural Changes in Monocrystalline Silicon Subjected to Nano-Indentation, Submitted to Tribology International (1998), in Preparation.

NII-Electronic Library Service